Available online at www.sciencedirect.com
SCIENCE DIRECT
ELSEVIER
International Journal of Mass Spectrometry 254 (2006) 53–62
International Journal of Mass Spectrometry
www.elsevier.com/locate/ijms

Ion trajectory simulations of axial ac dipolar excitation in the Orbitrap

Guangxiang Wu [a], Robert J. Noll [a,*], Wolfgang R. Plass [b], Qizhi Hu [a], Richard H. Perry [a], R. Graham Cooks [a,**]

[a] *Department of Chemistry, Purdue University, West Lafayette, IN 47907-2084, United States*
[b] *II. Physikalisches Institut, Justus-Liebig-Universität Giessen, Heinrich-Buff-Ring 16, 35392 Giessen, Germany*

Received 30 March 2006; received in revised form 5 May 2006; accepted 6 May 2006
Available online 12 June 2006

Abstract

The newly developed version of the multi-particle ion trajectory simulation program, ITSIM 6.0, was applied to simulate ac dipolar excitation of ion axial motion in the Orbitrap. The Orbitrap inner and outer electrodes were generated in AutoCAD, a 3D drawing program. The electrode geometry was imported into the 3D field solver COMSOL; the field array was then imported into ITSIM 6.0. Ion trajectories were calculated by solving Newton's equations using Runge–Kutta integration methods. Compared to the analytical solution, calculated radial components of the field at the device's "equator" ($z = 0$) were within 0.5% and calculated axial components midway between the inner and outer electrodes were within 0.2%.

The experiments simulated here involved the control of axial motion of ions in the Orbitrap by the application of dipolar ac signals to the split outer electrodes, as described in a recently published paper from this laboratory [Hu et al., J. Phys. Chem. A 110 (2006) 2682]. In these experiments, ac signal was applied at the axial resonant frequency of a selected ion. Axial excitation and eventual ion ejection resulted when the ac was in phase with, i.e., had 0° phase relative to ion axial motion. De-excitation of ion axial motion until the ions were at $z = 0$ and at rest with respect to the z-axis resulted if the applied ac was out of phase with ion motion, with re-excitation of ion axial motion occurring if the dipolar ac was continued beyond this point. Both de-excitation and re-excitation could be achieved mass-selectively and depended on the amplitude and duration (number of cycles) of the applied ac. The effects of ac amplitude, frequency, phase relative to ion motion, and bandwidth of applied waveform were simulated. All simulation results were compared directly with the experimental data and good agreement was observed. Such ion motion control experiments and their simulation provide the possibility to improve Orbitrap performance and to develop tandem mass spectrometry (MS/MS) capabilities inside the Orbitrap.

Keywords: Orbitrap; Field solver; Harmonic motion; Dipolar ac; Excitation; Mass spectrometry; Fourier transform; Ion trajectory simulation

1. Introduction

The Orbitrap as a new type of mass analyzer has drawn attention recently due to its high analytical performance and relatively small size [1–6]. It provides high mass resolution (up to 150,000), large space charge capacity, high mass accuracy (1–5 ppm), a mass/charge range of at least 6000 and a linear dynamic range greater than 1000. It has recently been reviewed [2]. The Orbitrap is a type of modified Kingdon trap [7] and consists of an outer barrel-like electrode and a coaxial inner spindle-like electrode, as shown in Fig. 1. During orbital trapping, a high negative dc voltage is applied to the inner electrode. Ions with high kinetic energy, ca. 1–2 keV, are injected perpendicularly to the main axis of the Orbitrap. Stable ion motion involves both orbiting motion around the central electrode (r, φ-motion, where φ designates angular position) and simultaneous oscillation along the z-axis. Only ions with appropriate tangential velocity achieve stable orbits around the inner electrode. The outer electrode is actually split at the equator ($z = 0$ plane), thus forming two half-electrodes, so that the image current induced by ion axial motion may be detected [3].

We have recently described experiments that have involved the control of axial motion of ions in the Orbitrap by the application of dipolar ac signals to the split outer electrodes [8]. The dipolar ac signal is applied to both halves of the split outer elec-

* Corresponding author. Tel.: +1 765 494 5265; fax: +1 765 494 9421.
** Corresponding author. Tel.: +1 765 494 5263; fax: +1 765 494 9421.
E-mail addresses: rnoll@purdue.edu (R.J. Noll), cooks@purdue.edu (R.G. Cooks).

1387-3806/$ – see front matter © 2006 Elsevier B.V. All rights reserved.
doi:10.1016/j.ijms.2006.05.007

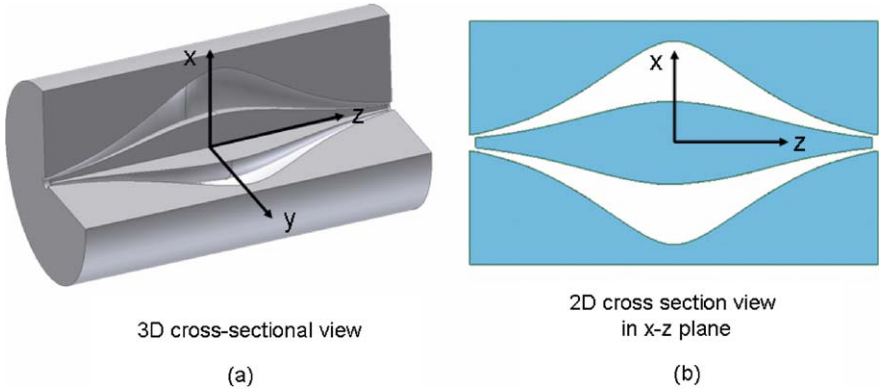

Fig. 1. The Orbitrap consists of two main electrodes. The outer electrode is barrel-shaped, while the coaxial inner electrode is spindle-shaped. (a) 3D view, (b) 2D cross-section view.

trode at the axial resonant frequency of a selected ion where there is a 180° phase difference between the two halves. It has been shown experimentally [8] that if the applied dipolar ac is in phase with, i.e., has 0° phase relative to ion axial motion, it will cause excitation of ion axial motion and eventual ejection from the trap. If the applied dipolar ac is out of phase with, i.e., has 180° phase relative to ion axial motion, it will first cause de-excitation of ion axial motion until the ions are at $z = 0$ and at rest with respect to the z-axis. If the dipolar ac is continued beyond this point, then re-excitation of ion axial motion can occur until eventually the ion is ejected from the trap. Both de-excitation and re-excitation can be achieved mass-selectively and depend on the amplitude and duration (number of cycles) of the applied ac. Such ion motion control experiments provide the possibility to improve Orbitrap performance and to develop tandem mass spectrometry (MS/MS) capabilities inside the Orbitrap.

Since Dawson performed the first ion calculations of ion motion in a pure quadrupole field [9], numerical simulations under varying conditions, including buffer gas collisions and space charge [10,11], non-linear fields and the influence of resonance excitation, have been pursued [12–16]. Tied closely to the development of mass spectrometry, numerical simulations have been demonstrated as an effective approach to explore ion trajectories in a variety of mass analyzers, including quadrupole ion traps [17], sector instruments [18], time-of-flight [19] and Fourier-transform ion cyclotron resonance (FT-ICR) [20,21]. Numerical simulations facilitate performance improvement in existing devices or to find new operating methods [22–24] and they also allow performance characteristics of as-yet-unbuilt instruments to be assessed and thus provide guidance for new and improved designs [25,26].

In this paper, the ion motion inside the Orbitrap due to axial ac dipolar excitation is simulated using the new version 6.0 of the Ion Trajectory SIMulation program, ITSIM [27]. Currently, ITSIM version 6.0 is still under development and, in contrast with its previous versions, has been adapted to allow interfacing with an external 3D field solver and can thus simulate ion trajectories inside electric/magnetic structures with fully arbitrary geometries. The overall simulation process using ITSIM 6.0 consists of four steps: (1) generating a 3D model of the structure to be used for simulation, (2) solving for the electric field inside the structure, (3) importing the calculated electric field into ITSIM 6.0 and (4) simulating ion motion under specified conditions.

2. Methods

2.1. Overview of ITSIM 6.0

ITSIM 6.0 allows the simulation of ion motion inside electrode structures with fully arbitrary geometries. A large number of ions, e.g., 10^4, can be simulated under user-defined experimental conditions. The electric potential distribution of the structure is calculated using a field solver program and the field is imported into ITSIM 6.0 as a potential array file or alternatively in the form of multipole expansion coefficients. The ions are generated in ion groups with user-defined physical properties, such as mass, charge, initial velocities and spatial coordinates, collision cross-section – including its dependence on collision energy – and background gas. Collections of ions can be given distributions of values of these parameters. Using scan tables, users can define any temporal sequence and magnitude of applied RF, ac, dc and arbitrary waveform voltages, which can be applied to the electrodes. The ion trajectories are calculated by numerically solving Newton's equations of motion with various Runge–Kutta (fourth, fifth or eighth order) integration methods with controlled (user-specified) step sizes. Ion-neutral collisions (elastic, inelastic and dissociative) and ion–ion space charge effects can be implemented in the simulations. Multiple data analysis functions can yield plots of electric fields, potentials and mass spectra obtained by both destructive or ion image current detection. Graphical output of one- and two-dimensional ion trajectory, velocity, energy and phase space is also available.

2.2. Field calculation and field accuracy

The shape of the two axially symmetric electrodes of the Orbitrap is defined by [3]:

$$z_{1,2}(r) = \sqrt{\frac{r^2}{2} - \frac{(R_{1,2})^2}{2} + (R_m)^2 \ln\left[\frac{R_{1,2}}{r}\right]} \quad (1)$$

where r is the radial coordinate, z the axial coordinate, indices 1 and 2 denote the central electrode and outer electrode, respectively, and $R_{1,2}$ denotes the maximum radius of the central or outer electrode ($R_1 = 4$ mm, $R_2 = 10$ mm). R_m is the characteristic radius; orbital (radial) trapping only takes place for ion trajectories with $r < R_m$. Since the Orbitrap has rotational symmetry about the z-axis, as shown in Fig. 1, the electric field between the inner and outer electrodes only needs to be calculated in the two-dimensional r–z plane ($r \geq 0$). Revolving the solution around the z-axis forms the corresponding three-dimensional field. Loosely speaking, a second symmetry element, the $z = 0$ plane, also exists and electric fields could be generated just in the first quadrant ($r \geq 0$, $z \geq 0$) in the r–z plane with reflection about $z = 0$ as well as rotation about $r = 0$ to generate the electrodes. However, the foregoing is true only if no dipolar excitations are used. In fact, due to the dipolar nature of the excitation waveforms, the $z = 0$ plane is, strictly speaking, not a symmetry element, and thus the regions on both sides of this plane must be used.

The shape of electrodes was first plotted in the r–z plane using AutoCAD software (Autodesk, Inc., US) with Eq. (1). Ideally, the Orbitrap electrodes extend infinitely, but as with both the quadrupole mass filter and the 3D quadrupole ion trap, the electrodes must be truncated at finite axial extent in a real device. As the exact position of truncation is proprietary and therefore unknown to us, we have chosen what must be a reasonable value and both electrodes are truncated at $z = \pm 11$ mm. The outer electrode is split into two electrodes at the equator ($z = 0$ plane) and the full gap width between the two separate outer electrodes was chosen as 0.1 mm. Once again, the actual gap width is proprietary and unknown to us and this represents a reasonable guess. The ion injection slot [3] was not modeled in this study.

The AutoCAD geometry file was then imported into the 3D field solver COMSOL 3.0a (COMSOL, Inc., US) where "Electrostatics" under "Axial symmetry (2D)" mode was chosen for the electric field calculations. Two sets of physical boundary conditions were defined to calculate (1) the electric field due to the central electrode dc voltage which was set to −1 V while the outer electrodes were kept grounded, and (2) the electric field due to the dipolar ac applied to the split outer electrodes, obtained by setting the left outer electrode to +1 V and the right outer electrode to −1 V with the central electrode kept grounded. During simulations, voltage amplitudes were applied to the central electrode (dc voltage) and the split outer electrodes (ac voltage) based on experimental conditions. In this paper, we will adopt the convention of reporting that the applied dipolar ac voltage V_{p-p} means that the voltage $+V_{p-p}$ is applied to one of the outer electrodes and that $-V_{p-p}$ is applied to the other outer electrode. An adaptive triangular mesh with maximum mesh element size 0.1 mm was applied inside the region enclosed by the two electrodes. This corresponds to the finest mesh density allowed by the memory size (3.0 GHz CPU and 3.0 GB RAM) of the desktop computer used. The electric field was then calculated over the triangular mesh by solving the Laplace equation. To reduce the computation time and memory requirement for the solution process, the "Direct linear system solver" was selected. The Orbitrap 2D mesh plot is shown in Fig. 2a and the calculated potential plot for the central electrode dc voltage is shown in Fig. 2b. The potential plot for the applied dipolar ac on the split outer electrodes is shown in Fig. 2c.

After the 2D field calculations, the electric field data in the r and z directions, $E_r(r,z)$ and $E_z(r,z)$, were exported into a text file on a regular grid and the grid size was chosen to sample 1000 data points in each direction for a total of 10^6 data points. The interface program CreatePot (written in-house) then converted the electric field into a field array file readable by ITSIM 6.0 and the ion trajectory calculations were pursued afterwards. Previously, the electric fields used for dipolar excitation with the split outer electrodes were calculated using a truncated multipole expansion (data not shown), yielding considerably weaker fields than those encountered in the actual device. The use, in this study, of a numerical potential array for the dipolar electric fields allows more accurate representation of these fields. The numerical field calculation was thus sought, which has resulted in considerably better agreement with experiment, as will be discussed later.

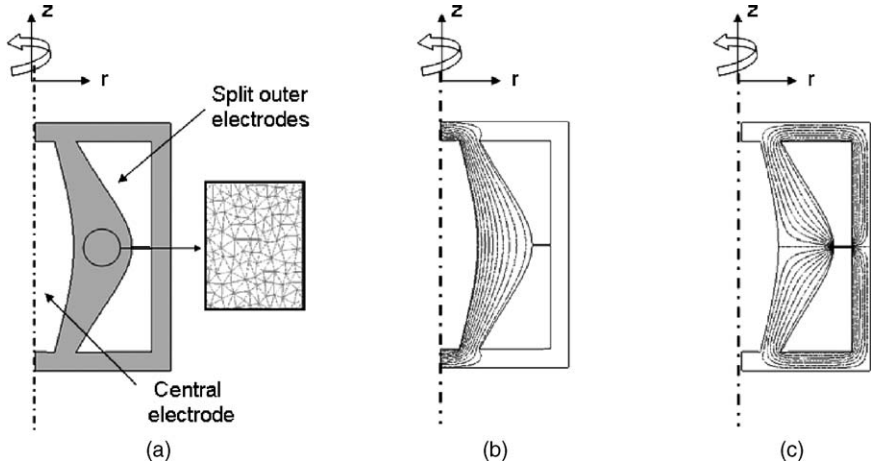

Fig. 2. Electric field calculated in the two-dimensional r–z plane of the Orbitrap using the COMSOL 3.0a program (COMSOL, Inc., US). (a) Triangular mesh plot, (b) plot of equipotential contours for a dc potential applied to the central electrode, (c) plot of equipotential contours for an applied dipolar potential (positive on left, negative on right) on the split outer electrodes.

To verify the accuracy of the field calculated from COMSOL 3.0a, the electric field was calculated for a more "ideal" Orbitrap geometry, where the outer electrode was not split at the equator but the electrodes were still truncated at $z = \pm 11$ mm. This field was compared with the analytical solution. Applying the dc voltage to the inner electrode with the outer electrode grounded, and recalling the potential distribution inside the Orbitrap:

$$U(r, z) = \frac{k}{2}\left(z^2 - \frac{r^2}{2}\right) + \frac{k}{2}(R_m)^2 \ln\left(\frac{r}{R_m}\right) + C \quad (2)$$

where k and C are constants; the electric field components in the r and z directions can be further derived as

$$E_r(r, z) = -\frac{\partial U}{\partial r} = \frac{k}{2}\left(r - \frac{(R_m)^2}{r}\right) \quad (3)$$

$$E_z(r, z) = -\frac{\partial U}{\partial z} = -kz \quad (4)$$

The radial electric field $E_r(r,z)$ at $z = 0$ and axial electric field $E_z(r,z)$ at $r = 7$ mm were calculated individually from COMSOL 3.0a. Comparison with the analytical solution shows good agreement: at any given point, the computed value of $E_r(r,z)$ at $z = 0$ is within 0.5% of the analytical solution Eq. (3) and for $E_z(r,z)$ at $r = 7$ mm, no point deviates more than 0.2% from the analytical solution Eq. (4).

3. Results and discussion

Ion trajectories were simulated for the Orbitrap using ITSIM 6.0. Unless indicated otherwise, for all simulations, ions started with the same initial spatial Gaussian distribution ($x = 7.0$ mm, $\sigma_x = 0.025$ mm; $y = 0$ mm, $\sigma_y = 0$; and $z = -4.5$ mm, $\sigma_z = 0.0625$ mm) with initial kinetic energy in the y direction (rotational velocity about the central electrode) $KE_y = 1730$ eV. The initial kinetic energies in the x and z directions, KE_x, KE_z were both zero. Axes are defined in Fig. 1. Axial motion is the basis for mass analysis in the Orbitrap. The potential in the z direction is quadratic and ion motion along the z-axis follows harmonic oscillation. The frequency of an harmonic oscillator is independent of ion kinetic energy and spatial distribution of ions. The oscillation frequency of ions along the z-axis inside the Orbitrap is given by the well-known harmonic oscillator result:

$$\omega_z = \sqrt{\frac{q}{m}k} \quad (5)$$

where q is the charge of the ion and m is the mass of the ion. The value for k may be obtained by solving Eq. (2) if the potential of the central electrode (V in Eq. (6) below) is known and the outer electrode is grounded:

$$k = \frac{V}{\left[\frac{1}{4}(R_2^2 - R_1^2) + \frac{1}{2}R_m^2 \ln\left(\frac{R_1}{R_2}\right)\right]} \quad (6)$$

Here, the other quantities have the same definitions as in Eq. (1).

In ITSIM 6.0, the inner electrode dc voltage was adjusted to −3308.75 V (compared with experimental dc voltage = −3300 V) to match the experimentally observed frequency for the $(MH)^+$ ion of reserpine (monoisotopic peak $m/z = 609.28$, corresponding to an axial harmonic oscillation frequency of 447.1825 kHz). Under such conditions, the reserpine frequency calculated from Eq. (5) above is 447.1821 kHz. The difference between the ITSIM result and the analytical value is only 0.0004 kHz which is well within the precision set by the choice of Fourier transform parameters in these simulations.

The simulated ion transient was obtained by collecting the differential ion image current from the two split outer electrodes as a function of time and then Fourier transformed using an FFT algorithm. Using Green's reciprocity theorem [28], one has

$$Q = -q\frac{\Delta\Phi(\mathbf{r})}{\Delta U} \quad (7)$$

where Q is the image charge induced on the electrode by a charge q at a position $\mathbf{r}$, and $\Delta\Phi(\mathbf{r})$ is the potential change induced at the same position $\mathbf{r}$ due to a voltage ΔU applied to the same electrode in the absence of any charge. Thus, the expression for ion image current for a single ion can be described in cylindrical coordinates as

$$I(t) = \frac{dQ}{dt} = -\frac{q}{\Delta U}\left[\frac{\partial\Delta\Phi(r, \varphi, z)}{\partial r}\dot{r} + \frac{\partial\Delta\Phi(r, \varphi, z)}{\partial\varphi}\dot{\varphi} + \frac{\partial\Delta\Phi(r, \varphi, z)}{\partial z}\dot{z}\right] \quad (8)$$

In ITSIM, this quantity can be rigorously calculated, as the partial derivatives in Eq. (8) are available from the numerical potential array. For a group of ions, the total image current will be the sum of individual currents given by Eq. (8).

Unless otherwise noted, total simulation time for simulated transients was 870 ms and the data acquisition period was from 30 to 870 ms. The sampling rate was 5000 kHz and the total number of data points collected was 2^{22} (4 M points) which nearly correspond to the experimental conditions. In the actual experiments, detection was delayed as much as 120 ms to allow stabilization of the central electrode power supply. To minimize the error accumulation during the ion trajectory integration, the fourth order Runge–Kutta integration method with integration step size 5 ns was chosen for all the simulations in this study. The test for oscillation amplitude conservation showed only a constant −0.02% deviation in z amplitude relative to the initial amplitude during the entire 870 ms simulation time. No collision and space charge effects were considered in the simulations.

3.1. Axial de-excitation/re-excitation and ejection

Axial de-excitation with subsequent re-excitation and ejection can be achieved by applying a dipolar ac on the split outer electrodes where the applied ac has a 180° phase relation with respect to ion axial motion. Ions whose mass-to-charge ratios are resonant with the applied ac will first experience a force in the direction opposite to their axial motion, causing their amplitude to decrease with the number of cycles of applied ac and diminishing to zero after an appropriate number of cycles. At this point, if the application of ac continues, their oscillation will fall into phase with the applied ac and their axial amplitude will

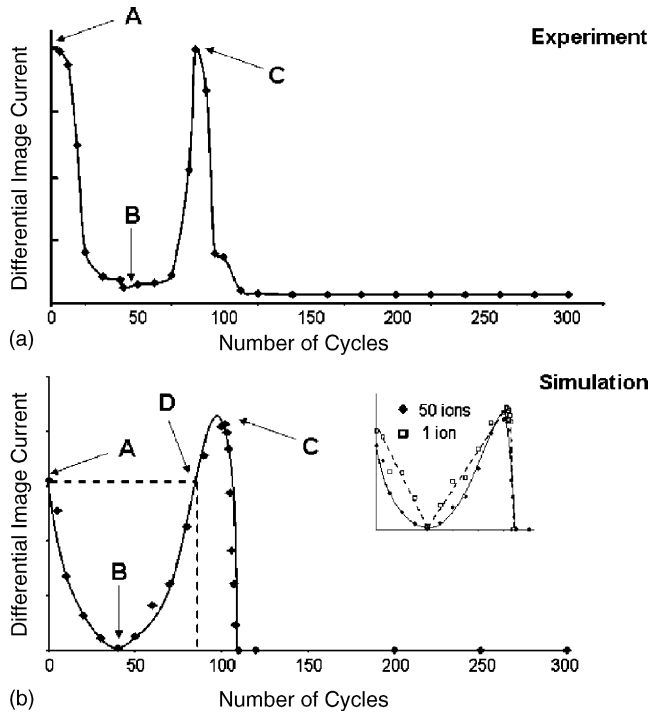

Fig. 3. Comparison of experimental and simulation for the de-excitation/re-excitation of reserpine ions at *m/z* 609.28. The resonant dipolar ac waveform was applied with 180° phase relative to ion axial motion. (a) Experimental de-excitation/re-excitation curve in which the intensity of the peak at *m/z* 609.28 is plotted as a function of the number of applied ac (20 V_{p-p}) cycles. Reprinted with permission from ref [8]. Copyright 2006 American Chemical Society. (b) Simulated de-excitation/re-excitation curve, the amplitude of the applied ac waveform is 16 V_{p-p}. The inset shows the effects of limited number of ions, single ion and 50 ions, used in simulations.

increase. Impact with the outer electrode can occur if the ac is applied for long enough. The experimental data was collected for reserpine (MH^+) ions, with monoisotopic peak at *m/z* 609.28 and $^{13}C_1$ isotopic peak at *m/z* 610.28. Shown in Fig. 3 is a comparison of the experimental (Fig. 3a) and simulated (Fig. 3b) ion signal of *m/z* 609.28 ions as a function of the number of ac cycles applied [8]. For the experimental data, each point on the curve was obtained by recording a separate transient. The applied ac waveforms had amplitudes of 20 V_{p-p} and frequency 447.2 kHz which matches the frequency of harmonic motion along the *z*-axis for the *m/z* 609.28 ion. The ion signal drops initially, reaching a minimum at about 42 cycles (point B), and then starts to rise again. At 84 cycles (point C), the signal reaches a maximum and then diminishes quickly to zero.

The experimental results were quantitatively simulated with two groups of ions, 50 ions of *m/z* 609.28 and 19 ions of *m/z* 610.28. The number of ions chosen was based on two factors. First, this ratio corresponds to the natural relative abundance between the monoisotopic peak of reserpine at *m/z* 609.28 and the $^{13}C_1$ isotope peak at 610.28. Secondly, this number of ions is a reasonable compromise between enough ions to provide "averaging" results on the one hand and few enough ions to provide relatively light demands computationally. In the simulation, the applied dipolar ac had amplitude 16 V_{p-p}, frequency 447.2 kHz, and 180° phase relative to ion axial motion. The applied ac amplitude (16 V_{p-p}) was deliberately chosen to be different from the experimental condition (20 V_{p-p}); and the discrepancy is due to systematic error in the experimental ac voltage. As shown in Fig. 3b, the simulated ion signal of *m/z* 609.28 ions drops initially, reaching a minimum at about 40 cycles (point B), and then starts to rise again. At 102 cycles (point C), the signal reaches a maximum and then diminishes quickly to zero. The smooth curve shown here is to guide the viewer's eye through the simulated data points.

The inset of Fig. 3b shows these results as well as the resulting curve for simulations for a single ion. The comparison between the single-ion and 50-ion simulations qualitatively illustrate the statistical error caused by the limited number of ions used in the simulation. As the number of ions is increased, the simulated plot agrees better with the experimental data. Furthermore, the main area of improvement is in the neighborhood around point B. Apparently, as more ions are included in the calculation, small differences in initial position will counter each other more effectively. Moreover, it seems as this effect is more noticeable when the ions have smaller axial amplitudes. Compared with experimental data, it takes approximately the same number of cycles to re-excite the ion signal back to the initial amplitude (point D, 87 cycles). However, there is a appreciable shift in the number of ac cycles required for the signal to reach the maximum (point C, 102 cycles). Comparison of Fig. 3a and b also shows that the ions are more rapidly ejected in the experiment than in the simulation. The reason for this difference is still not clear, although it may be due to the initial ion distribution used in the simulation. The ion packet in the experiment may actually occupy a distribution of axial positions sufficiently large (but not random) that the ac signal causes a fraction of the ions to be ejected almost immediately after point A. This loss of ions could then offset any gain in image signal due to the ions' larger axial amplitude upon re-excitation past point D.

Compared in Fig. 4 are the experimental (Fig. 4a) and simulated (Fig. 4b) mass spectra of *m/z* 609.28 and 610.28 ions corresponding to points A, B and C in Fig. 3. Note that the ion intensity is plotted as a function of axial frequency, rather than mass/charge, to allow the reader to gauge agreement between experiment and simulation for this quantity as well. In the experimental data, Fig. 4a, both *m/z* 609.28 (ω_z = 447.2 kHz) and *m/z* 610.28 (ω_z = 446.8 kHz) ions were de-excited simultaneously at point B. This is possible because of the broad bandwidth of the applied ac, 10 kHz. A tuned narrow bandwidth ac waveform (lower ac amplitude and larger number of ac cycles applied) should only de-excite *m/z* 609.28 ions and leave *m/z* 610.28 ions unaffected, as described below.

In the simulated mass spectra, Fig. 4b, signal intensities for both *m/z* 609.28 and 610.28 were de-excited at 40 cycles and re-excited at 102 cycles. For the simulated point B, the ion peak height at *m/z* 609.28 is approximately 1% of the original ion peak height at point A. This compares well with experiment, where the peak height for *m/z* 609.28 drops to approximately 6% of its original ion peak height at point A. We note that baseline noise level on the mass spectrum corresponding to point A is about 1%, so experimentally, de-excitation to this level is indistinguishable from complete de-excitation.

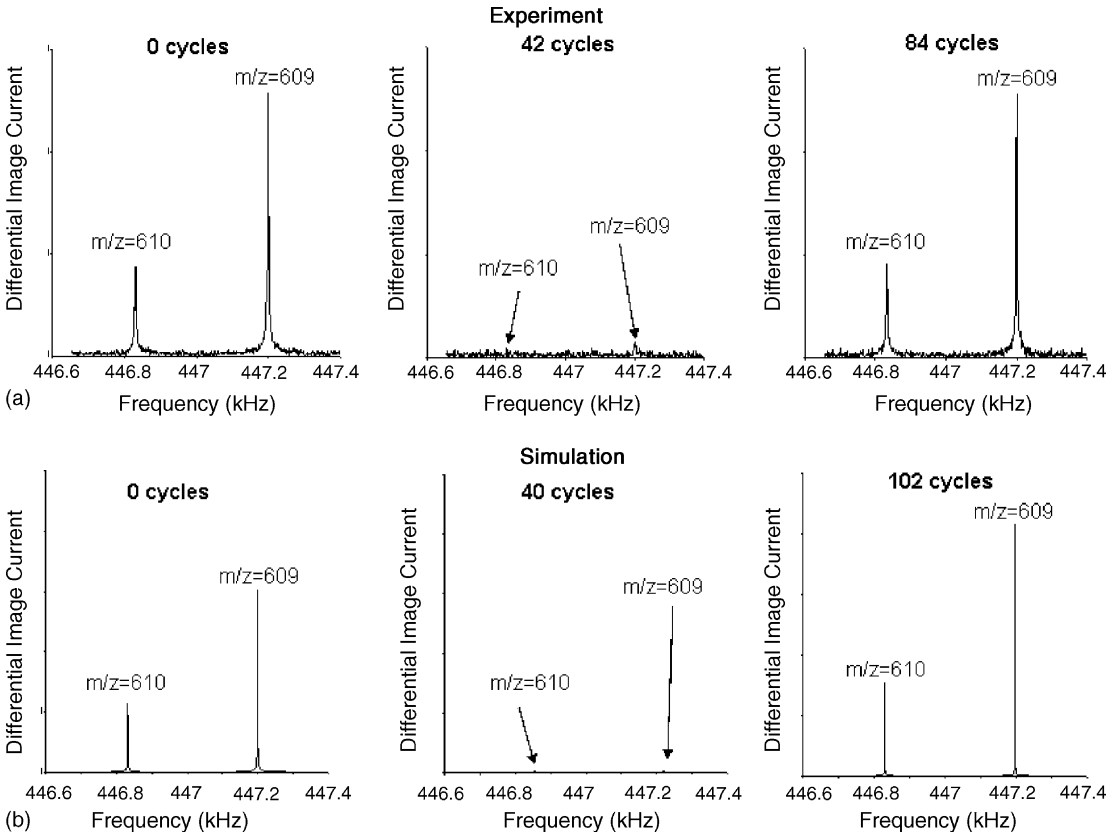

Fig. 4. Comparison of experimental and simulated mass spectra in the de-excitation/re-excitation of reserpine ions at *m/z* 609.28. The resonant dipolar ac waveform was applied 180° relative to ion axial motion. (a) Experimental spectra, corresponding to points A (the normal Orbitrap mass spectrum without applied ac), B (the fully de-excited mass spectrum) and C (the fully re-excited mass spectrum) on the de-excitation/re-excitation curve Fig. 3a. Reprinted with permission from ref [8]. Copyright 2006 American Chemical Society. (b) Simulated spectra, corresponding to points A (the normal Orbitrap mass spectrum without applied ac), B (the fully de-excited mass spectrum) and C (the fully re-excited mass spectrum) on the de-excitation/re-excitation curve Fig. 3b.

3.2. Resonance curves and effect of ac bandwidth

Fig. 5 illustrates both simulated and experimental resonance curves for two isotopic peaks of reserpine at *m/z* 609.28 and 610.28. The signal intensity for each isotopic ion is plotted as a function of applied ac frequency which has constant amplitude and 180° initial phase relative to ion axial motion. For each curve, the number of ac cycles applied was held constant and corresponds to the full de-excitation of ions at exact resonance. Fig. 5a and b show the experimental resonance curves at two different ac conditions. In Fig. 5a, the ac amplitude was 3.8 V_{p-p} and the number of cycles applied was 250. With larger ac amplitude, fewer cycles are needed to achieve de-excitation and thus the bandwidth is much wider. The resonance peaks of the ions at *m/z* 609.28 and 610.28 overlap substantially with each other and thus poor resolution results.

In Fig. 5b, the ac amplitude was 0.16 V_{p-p} and the number of cycles applied was 5500. Applying an ac waveform with a lower amplitude results in needing a greater number of ac cycles in the time domain, but also results in a narrower excitation bandwidth in the frequency domain. Thus, with lower ac amplitude, the resonance peaks of the two ions are well separated, with center frequencies of 447.2 kHz for *m/z* 609.28 and 446.8 kHz for *m/z* 610.28.

Fig. 5c and d show the corresponding simulated resonance curves using an ac waveform of 3.04 V_{p-p} amplitude and 200 cycles (Fig. 5c) and amplitude 0.128 V_{p-p} and 4000 cycles (Fig. 5d). Good qualitative agreement exists between experiment and simulation. For larger ac amplitudes, the resonances for the two isotopes overlap for both experiment and simulation; in the case of smaller ac amplitude, the resonances are well-separated. However, at both low and high ac amplitude, the widths (as measured at FWHM) of the experimental resonances (0.19 and 8.3 kHz, respectively) are twice those of the simulated resonances (0.07 and 3.8 kHz). Moreover, the ac bandwidth for the simulations are slightly *larger* than experiment at both lesser ac amplitude (0.22 kHz for the simulation versus 0.16 kHz for experiment) and greater ac amplitude (4.5 kHz versus 3.6 kHz). Presumably, the experimental resonances would thus be somewhat wider had they been acquired using the same ac bandwidths as those of the simulations.

The mostly likely explanation for the broadening of the experimental resonances would be the distribution of ion axial phases relative to the applied ac. Only when ion motion is 180° relative to the applied ac will complete axial de-excitation occur. This suggests that the discrepancy between experiment and simulation is due to choosing too small an axial distribution for the initial conditions of the simulation. Additionally, in the exper-

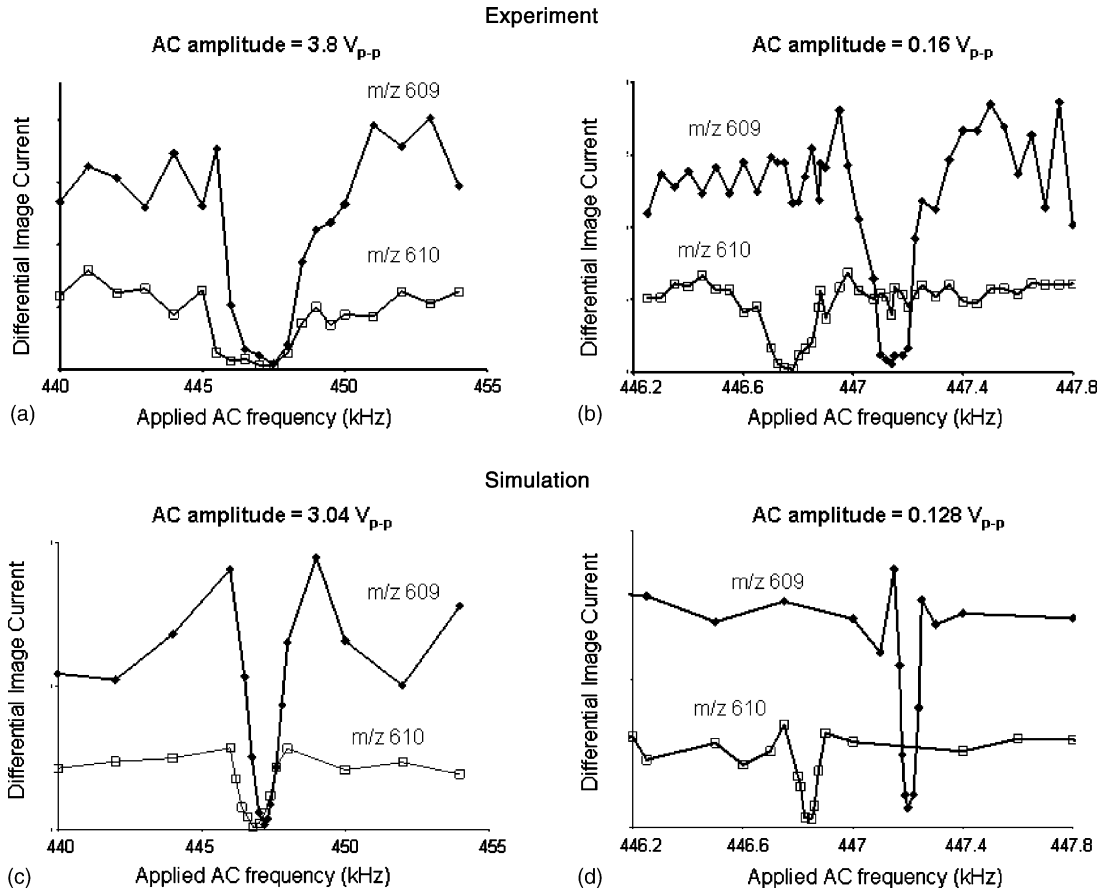

Fig. 5. Simulated and experimental resonance curves of the monoisotopic and $^{13}C_1$ reserpine ions at *m/z* 609.28 and 610.28. The applied dipolar ac waveform has 180° phase relative to the ion axial motion. Experimental resonance curves were obtained using (a) broadband ac waveform (3.8 V_{p-p}, 250 cycles) and (b) narrowband ac waveform (0.16 V_{p-p}, 5500 cycles). Reprinted with permission from ref [8]. Copyright 2006 American Chemical Society. Simulated resonance curves using (c) broadband ac waveform (3.04 V_{p-p}, 200 cycles) and (d) narrowband ac waveform (0.128 V_{p-p}, 4000 cycles).

iment, field imperfections and ion collisions with background gas molecules may also serve to broaden the ion axial phase distribution of the ions and are not taken into account in our simulations. The use of too few ions in the simulation may also play a role as well. The role of ion–ion interactions, viz., space charge effects in the experiments cannot be completely ruled out either.

3.3. Mass-selective de-excitation/re-excitation and ejection

Depicted in Fig. 6 are the experimental (Fig. 6a–c) and simulated (Fig. 6d–f) mass spectra of the isotope-selective de-excitation and re-excitation of *m/z* 609.28. In the experimental mass spectra, the applied dipolar ac had amplitude 0.16 V_{p-p} and was applied for 5500 cycles, resulting in a bandwidth of 0.16 kHz, smaller than the difference of 0.4 kHz between the two isotope peaks. At 5500 cycles, the signal at *m/z* 609.28 drops to baseline without apparently disturbing the peak at *m/z* 610.28. After the application of an additional 5550 cycles, for a total of 11,000 applied cycles, the signal at *m/z* 609.28 is re-excited to its initial amplitude. Careful observers will note that the peak heights in Fig. 6a and c are not exactly the same. This is because each mass spectrum was acquired separately (viz. are different ion populations) and the differences in height correspond to experimental fluctuation in the ESI source.

The corresponding simulations (Fig. 6d–f) of mass-selective de-excitation and re-excitation of the *m/z* 609.28 ions are consistent with experimental results. However, the simulated dipolar ac had a lower amplitude of 0.128 V_{p-p} compared with the experimental value of 0.16 V_{p-p}. Once again, this difference is due to systematic error in the experimental ac amplitude. Thus the number of cycles applied to reach full de-excitation and re-excitation of *m/z* 609.28 ion differs from the experimental results: de-excitation at 4000 cycles in the simulation compared with 5500 in the experiment, re-excitation at 12,100 cycles (to the maximal extent, point C in Fig. 3b) in the simulation compared with 11,000 in the experiment. As described above, the discrepancy may still be due to different initial ion distributions in the simulation versus experiment.

Fig. 7 illustrates the comparison of simulations and experiments of mass-selective de-excitation/re-excitation performed in a more integrated fashion. In the experiment, ions of singly-charged reserpine $(MH)^+$ at *m/z* 609.28 were de-excited and re-excited in the presence of doubly charged angiotensin $(MH_2)^{2+}$ ions at *m/z* 649.35 by applying two identical ac waveforms (447.2 kHz, 3.8 V_{p-p}, 250 cycles each, 0.56 ms) 100 and 340 ms after image current detection was started. Detection continued

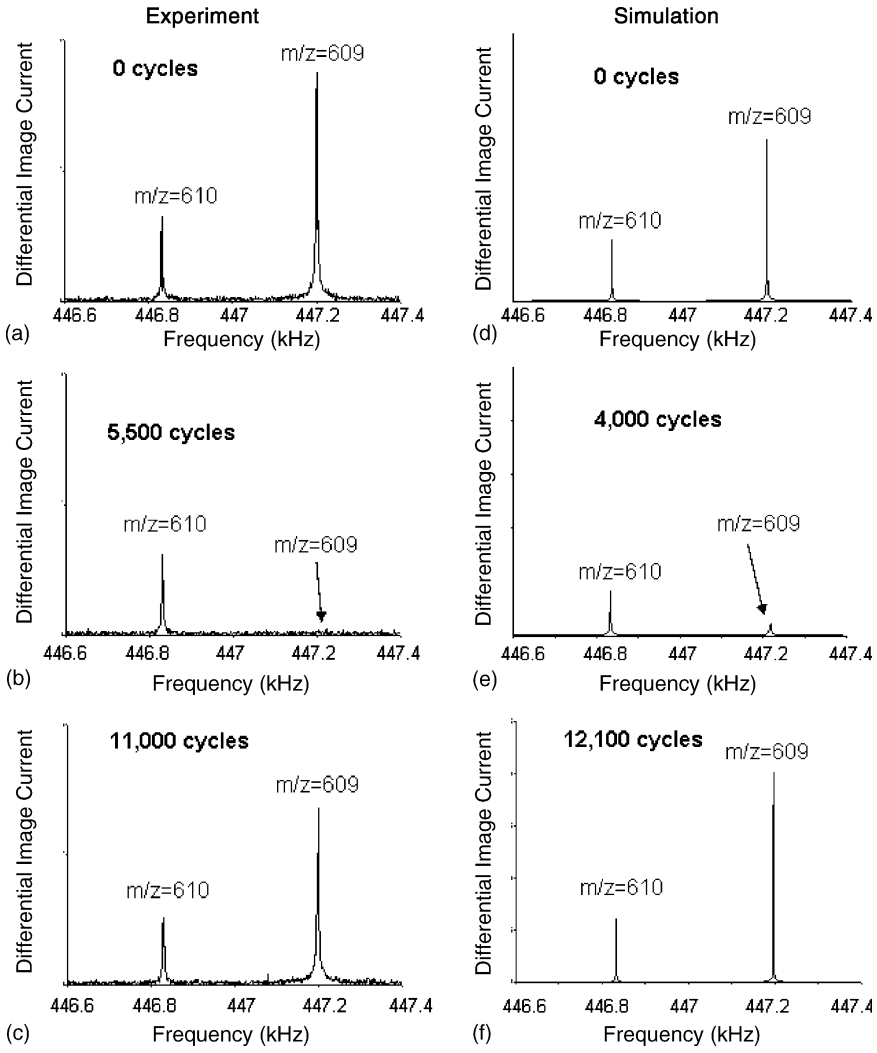

Fig. 6. Comparison of simulated and experimental mass-selective de-excitation/re-excitation mass spectra. The monoisotopic ions of reserpine at *m/z* 609.28 can be de-excited and re-excited without affecting the isotopic ion population at *m/z* 610.28 using a low amplitude, narrow bandwidth dipolar ac waveform. The applied ac has 180° phase relative to ion axial motion. Experimental spectra with applied ac amplitude 0.16 V_{p-p} and duration times: (a) 0 cycles, b) 5500 cycles and (c) 11,000 cycles. Reprinted with permission from ref [8]. Copyright 2006 American Chemical Society. Simulated spectra with applied ac amplitude 0.128 V_{p-p} and duration times: (d) 0 cycles, (e) 4000 cycles and (f) 12,100 cycles.

for 800 ms. The experimental transient is shown in Fig. 7a. The three transient regions (A, B and C in Fig. 7a) were individually Fourier transformed. The experimental mass spectra are shown in Fig. 7b–d which correspond to the transient regions A, B and C, respectively. It can be clearly seen that, after applying the first ac waveform, the reserpine ions have nearly completely disappeared, corresponding to de-excitation of the ions to the equatorial plane of the Orbitrap. By applying the second ac waveform, the reserpine ions were re-excited to regain the original peak intensity. During the entire experiment, the angiotensin ions were unaffected.

In the simulations, two groups of ions, 50 ions for reserpine *m/z* 609.28 and 106 ions for doubly charged angiotensin *m/z* 649.35, were simulated. The two ac waveforms (both 3.04 V_{p-p}, 447.2 kHz) were applied for 200 cycles each, i.e., 0.447 ms. The simulated spectra are shown in Fig. 7e–g, corresponding to the transient regions A, B and C, respectively. The mass spectra corresponding to these regions were obtained by separate simulations. In all three cases, 2^{19} sampling data points for 90 ms were acquired and then Fourier transformed. For Fig. 7e, before application of the first ac waveform, the total simulation time was 100 ms and the data acquisition period for transient region A was from 0 to 90 ms. For Fig. 7f, ion motion was simulated for region A, the first ac waveform, and region B of the transient. Thus, the total simulation time for this mass spectrum was 340 ms. The first ac waveform was applied at 100 ms into the simulation. The data acquisition period was from 100.447 to 190.447 ms, viz., for the 90 ms immediately following application of the first ac waveform. The starting relative phase of the applied dipolar ac waveform was adjusted by delaying 0.223 μs (1/10 ac cycle) in order to maintain the exact 180° phase relative to ion axial motion. For Fig. 7g, ion motion was run for regions A–C, and the two periods of ac waveform application, for a total of 800 ms simulated time. The second ac waveform was applied at 340 ms

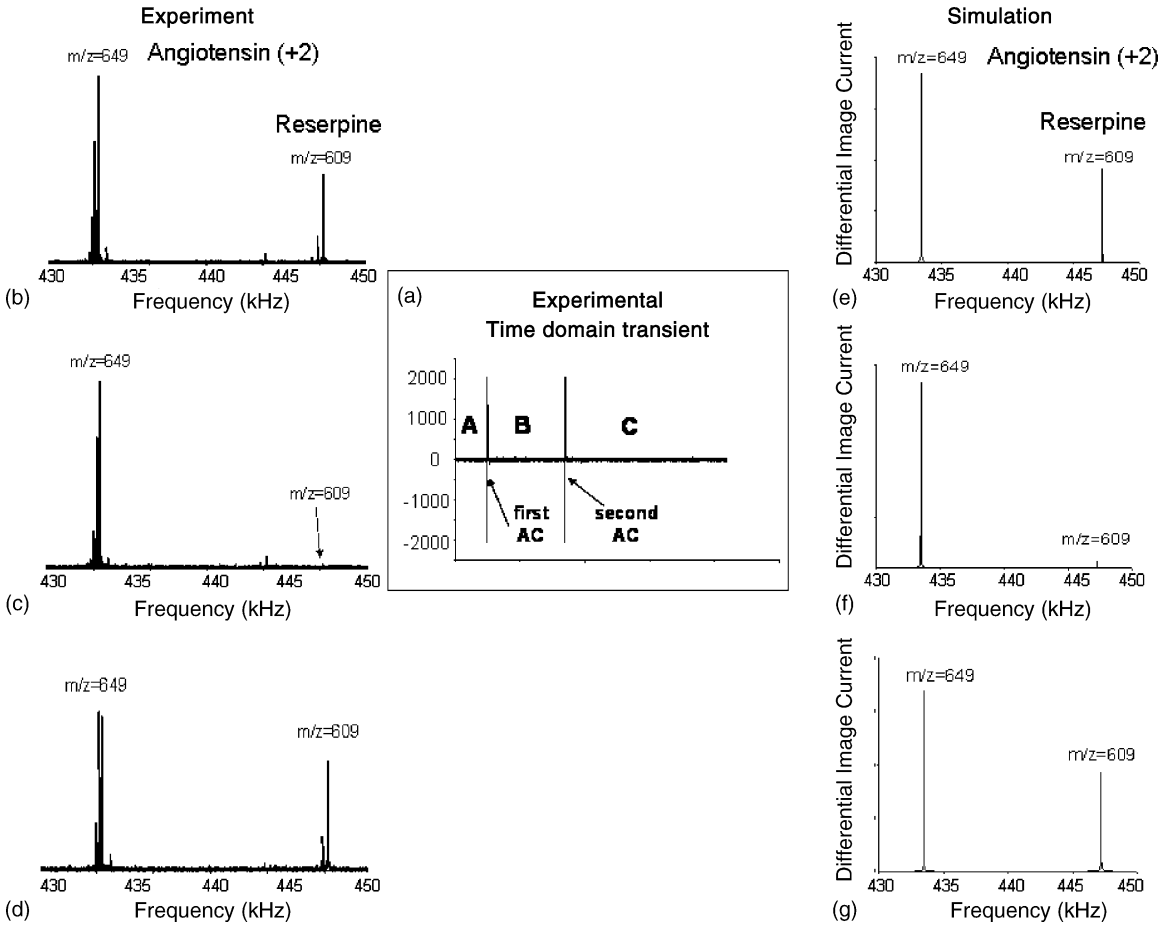

Fig. 7. Simulation and experimental results for the mass-selective de-excitation/re-excitation of reserpine ions at *m/z* 609 without affecting doubly charged angiotensin ions at *m/z* 649. (a) The experimental transient shows the separate application of two dipolar ac waveforms (447.2 kHz, 3.8 V_{p-p}, 250 cycles each) after image current detection was started. (b) Experimental mass spectrum obtained for transient region A, showing peaks for angiotensin (MH_2^{2+} at *m/z* 649) and reserpine (MH^+ at *m/z* 609). (c) De-excitation of reserpine ions to noise level in transient region B. (d) Re-excitation of reserpine ions in transient region C. Reprinted with permission from ref [8]. Copyright 2006 American Chemical Society. (e–g) Corresponding simulated mass spectra, with two separate dipolar ac waveforms applied (447.2 kHz, 3.04 V_{p-p}, 200 cycles each) with timing as in the experiment.

after the start of the simulation. Data acquisition took place in region C, from 340.447 to 430.447 ms. It can be seen clearly that the ions for reserpine *m/z* 609.28 were de-excited almost completely after applying the first ac waveform and were re-excited after applying with the second ac waveform. The simulation results are consistent with the experimental results.

3.4. Excitation/ejection

If the dipolar ac waveform applied to the split outer electrodes of the Orbitrap is in phase with, i.e., has 0° phase relative to the ion axial motion, the ions will be excited to higher amplitude and eventually be ejected from the Orbitrap if they acquire sufficient energy. The comparison of simulated and experimental results is shown in Fig. 8. The peak intensity of reserpine ions *m/z* 609.28 was collected experimentally (Fig. 8a) as a function of number of ac cycles. The applied ac waveform had 3.8 V_{p-p} amplitude and 447.2 kHz frequency. The peak intensity decreases immediately and very rapidly with increasing number of applied ac cycles. Fig. 8b shows the corresponding simulation result where 50 ions for reserpine *m/z* 609.28 were simulated with applied dipolar ac of 3.04 V_{p-p}, 447.2 kHz, and in phase relative to the phase of the ions. The ion signal increases initially, reaching a maximum at about 100 cycles, and then starts to drop abruptly to zero. A smoothed curve is also shown here to guide the viewer's eye through the simulated data points.

Although the experimental results are reasonably well modeled, important qualitative and quantitative differences remain. The foremost difference is that, in the simulation, ion intensity increases by approximately 50% before decreasing, whereas in the experiment, ion signal decreases monotonically from zero cycles of ac. This suggests that the experimental ion packet is considerably wider axially than as simulated. It is possible that ejection of ions from the Orbitrap (and thus loss of ion signal) occurs nearly immediately upon application of the ac. Additionally, in the simulation, the increase in peak intensity between 0 and 100 cycles is not monotonic. This suggests the possibility that the details of averaging of ion image signals in the simulation is highly dependent upon the exact details of the dynamic evolution of the ion population.

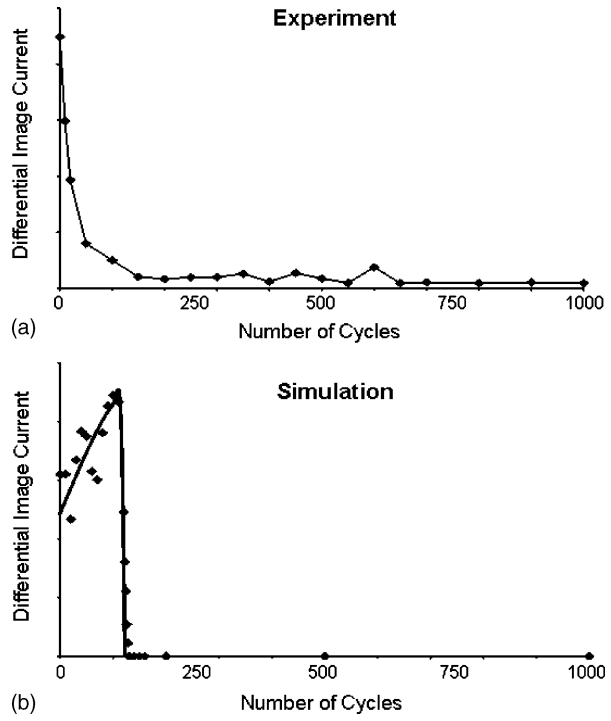

Fig. 8. Experimental and simulated plots of ion signal vs. number of applied cycles of dipolar excitation for the direct ejection of reserpine ions at *m/z* 609. The resonant dipolar ac waveform was applied in phase with ion axial motion. (a) Experimental excitation/ejection curve (applied ac amplitude = 3.8 V_{p-p}). Reprinted with permission from ref [8]. Copyright 2006 American Chemical Society. (b) Simulated excitation/ejection curve (applied ac amplitude = 3.04 V_{p-p}).

4. Conclusions

This paper describes simulation of axial ac dipolar excitation in the Orbitrap obtained using the newly developed ITSIM 6.0. This paper also represents the first application of ITSIM 6.0 to an electrostatic mass analyzer. The electric fields due to the dc voltage applied to the central electrode and the dipolar ac waveform applied to the split outer electrodes were calculated directly by using the finite element field solver COMSOL 3.0a. The simulation results agree quite well with the experimental data. However, a discrepancy does exist with respect to the applied dipolar ac amplitude; it is believed most likely due to the systematic error of measuring the experimental ac voltage. Additionally, the ion ejection process, whether by direct excitation or de-excitation/re-excitation, appears to be more rapid than our simulations show; the initial ion distribution may be a crude approximation of the actual experiment. The effects of initial ion spatial and velocity distributions, the limited number of ions simulated, and not including the ion injection slot in the model may contribute to inconsistencies between simulation and experiment. Nevertheless, the simulations obtained using ITSIM 6.0 have been qualitatively correct and quantitatively correct in most aspects. Such simulations, in addition to gaining physical insight into ions' behavior inside the mass analyzer, may also be useful in designing new modes of operation. This includes the effect of different types of excitation functions, such as square pulses, and – in addition to the dipolar excitations described here – different types of accelerating fields, such as parametric excitations.

Acknowledgements

The authors acknowledge support from NSF Major Research Instrumentation (MRI) program (CHE-0216239), the Office of Naval Research (ONR) program (N00014-02-1-0834), and Thermo Electron Corporation. We also acknowledge Benjamin B. Fabian for valuable discussions about COMSOL modeling.

References

[1] M. Hardman, A. Makarov, Anal. Chem. 75 (2003) 1699.
[2] Q. Hu, R.J. Noll, H. Li, A. Makarov, M. Hardman, R.G. Cooks, J. Mass Spectrom. 40 (2005) 430.
[3] A. Makarov, Anal. Chem. 72 (2000) 1156.
[4] M. Thevis, A. Makarov, S. Horning, W. Schanzer, Rapid Commun. Mass Spectrom. 19 (2005) 3369.
[5] J.R. Yates, D. Cociorva, L. Liao, V. Zabrouskov, Anal. Chem. 78 (2006) 493.
[6] S.M. Peterman, N. Duczak Jr., A.S. Kalgutkar, M.E. Lame, J.R. Soglia, J. Am. Soc. Mass Spectrom. 17 (2006) 363.
[7] K.H. Kingdon, Phys. Rev. 21 (1923) 408.
[8] Q. Hu, A. Makarov, R.G. Cooks, R.J. Noll, J. Phys. Chem. A 110 (2006) 2682.
[9] P.H. Dawson, N.R. Whetten, J. Vac. Sci. Technol. 5 (1968) 91.
[10] F. Vedel, J. Andre, M. Vedel, G. Brincourt, Phys. Rev. A 27 (1983) 2321.
[11] F. Vedel, J. Andre, Phys. Rev. A 29 (1984) 2098.
[12] F.A. Londry, G.J. Wells, R.E. March, Rapid Commun. Mass Spectrom. 7 (1993) 43.
[13] S. Sevugarajan, A.G. Menon, Int. J. Mass Spectrom. 197 (2000) 263.
[14] M. Sudakov, Int. J. Mass Spectrom. 206 (2001) 27.
[15] J. Franzen, Int. J. Mass Spectrom. Ion Process. 106 (1991) 63.
[16] R.E. March, J.F.J. Todd (Eds.), Practical Aspects of Ion Trap Mass Spectrometry, Fundamentals of Ion Trap Mass Spectrometry, vol. I, CRC Press, Boca Raton, FL, 1995 (Chapter 3).
[17] R.E. March, Rapid Commun. Mass Spectrom. 12 (1998) 1543.
[18] J.A. Diaz, C.F. Giese, W.R. Gentry, J. Am. Soc. Mass Spectrom. 12 (2001) 619.
[19] C. Marinach, A. Brunot, C. Beaugrand, G. Bolbach, J.C. Tabet, Int. J. Mass Spectrom. 213 (2002) 45.
[20] D.W. Mitchell, J. Am. Soc. Mass Spectrom. 10 (1999) 136.
[21] X. Xiang, S. Guan, A.G. Marshall, J. Am. Soc. Mass Spectrom. 5 (1994) 238.
[22] L. Ding, M. Sudakov, S. Kumashiro, Int. J. Mass Spectrom. 221 (2002) 117.
[23] G. Wu, R.G. Cooks, Z. Ouyang, Int. J. Mass Spectrom. 241 (2005) 119.
[24] B.E. Wilcox, C.L. Hendrickson, A.G. Marshall, J. Am. Soc. Mass Spectrom. 13 (2002) 1304.
[25] D.E. Austin, D. Cruz, M.G. Blain, J. Am. Soc. Mass Spectrom. 17 (2006) 430.
[26] M.G. Blain, L.S. Riter, D. Cruz, D.E. Austin, G. Wu, W.R. Plass, R.G. Cooks, Int. J. Mass Spectrom. 236 (2004) 91.
[27] G. Wu, M. Yu, W.J. Chappell, R.G. Cooks, W.R. Plass, Z. Ouyang, J. Am. Soc. Mass Spectrom. (submitted for publication).
[28] J.A. Marto, A.G. Marshall, L. Schweikhard, Int. J. Mass Spectrom. Ion Process. 137 (1994) 9.